metals

MDPI

Article

Microstructure and Performance Analysis of Welded Joint of Spray-Deposited 2195 Al-Cu-Li Alloy Using GTAW

Chuanguang Luo [1,2], Huan Li [1], Yonglun Song [3,*], Lijun Yang [1,*] and Yuanhua Wen [2]

[1] Tianjin Key Laboratory of Advanced Joining Technology, Tianjin University, Tianjin 300072, China; chg_luo@163.com (C.L.); lihuan@tju.edu.cn (H.L.)
[2] Sichuan Aerospace Changzheng Equipment Manufacturing Co., Ltd., Chengdu 610100, China; wyh20017@163.com
[3] College of Mechanical Engineering and Applied Electronics Technology, Beijing University of Technology, Beijing 100124, China
* Correspondence: 13911138686@163.com (Y.S.); yljabc@tju.edu.cn (L.Y.); Tel.: +86-13911138686 (Y.S.); +86-13002244217 (L.Y.)

Received: 26 July 2020; Accepted: 9 September 2020; Published: 14 September 2020

Abstract: High-strength aluminum alloy fabricated using spray deposition technology possesses many advantages, such as fine crystal grains, low component segregation, uniform microstructure, and small internal stress. In this study, spray-deposited 2195 Al-Cu-Li alloy in forged state was used and welded using the gas tungsten arc welding (GTAW) process to test and verify the features of the fusion joint. Quantitative analysis was carried out to evaluate the relationship between the local microstructures and performances of the fusion joint, which was composed of four zones: weld metal, fusion zone, heat-affected zone, and base metal. The characteristic quantities of each zone, including recrystallized grain fraction, grain sizes, grain misorientation angle, and Vickers hardness, and their distributions were considered as the key factors affecting the performance of the joint because of welding thermal cycle impact on the fusion joint. To recognize the metallurgical characteristics of spray-deposited alloy 2195, a statistical algorithm based on the concept of the Hall–Petch relationship was proposed to validate the actual test results, which include the correlation effects of both the filler wire and welding process. The correlation between the microstructures and performances of several characteristic quantities were evaluated by integrating the above characteristic information of the fusion joint under the strong coupling of multiple factors. Thus, the advantages of weldability of spray-deposited alloy 2195 using GTAW could be understood in detail.

Keywords: spray-deposited Al-Cu-Li alloy; GTAW; microstructure; welded joint; performance analysis

1. Introduction

Al-Cu-Li alloy is a new high-strength material that possesses low density and high elasticity. It is in increasing demand by the manufacturers of structural parts for aerospace applications. Alloy 2195, which belongs to the Al-Cu-Li-Ag-Mg series, has been used in lightweight fuel tank structural parts of aerospace vehicles [1–5]. In this application, the cylinder and vessel head are welded with bending rolled plates after spin forming, whereas the connectors such as flanges and connecting rings formed by forging are assembled and welded to these parts. Fabrication of these parts through traditional melt casting and forging often result in defects such as component segregation, oxide inclusion, delayed cracking, and large residual stress. Furthermore, joint cracks in welded forging flanges occur frequently. Cracking occurs mostly on the side of the fusion zone and is closely related to the

metallurgical defects of forging materials. These problems have been proved to be detrimental to aerospace vehicle tank structures [6].

High-strength Al alloy fabricated using spray deposition possesses many advantages [7–10], such as fine crystal grains, low component segregation, uniform structure, and small internal stress, as well as short production cycle. Spray deposition is performed under vacuum or an inert gas protection atmosphere to ensure that the work pieces have low oxygen content and less oxide inclusions, and it is conducive to subsequent thermal processing. Furthermore, the machining allowance of forgings and annular parts can be significantly reduced.

In this study, forged plates of spray-deposited alloy 2195 were welded using the gas tungsten arc welding (GTAW) process to test and observe the characteristics of the fusion joint. Because of the impact of the welding thermal cycle on the fusion joint, it was composed of four zones: weld metal (WM), fusion zone (FZ), heat-affected zone (HAZ), and base metal (BM). The characteristic quantities of each zone, including the recrystallized grain fraction, grain sizes, grain misorientation angle, and Vickers hardness, and their distributions were considered as the key factors affecting the performance of the joint because of the impact of the welding thermal cycle on the fusion joint. To recognize the metallurgical characteristics of spray-deposited alloy 2195, a statistical algorithm based on the concept of the Hall–Petch relationship was proposed to validate the actual test results, which include the correlation effects of both the filler wire and welding process. The correlation between the microstructures and performances of several characteristic quantities was evaluated by integrating the above characteristic information of the fusion joint under the strong coupling of multiple factors. Thus, the advantages of weldability of spray-deposited alloy 2195 using GTAW could be understood in detail.

2. Experimental Procedure

2.1. Materials

In this study, cylindrical blanks of the spray-deposited alloy 2195 (designation: D2195; manufacturer: Jiangsu HR Spray Forming Alloy Co., Ltd., Zhenjiang, China) were Φ 300 mm in diameter. The blanks were cogged and forged into pieces (size: 300 mm × 300 mm × 60 mm), sequentially annealed at 425 °C for 2 h, cooled in the furnace for 35–40 min, and then cooled in air. The solution was treated at 505 °C for 70 min in a protection atmosphere furnace, with the time of quenching transfer to water being less than 3 s, and quenched in water at not more than 20 °C, and the cooling rate was approximately 120 °C/s. This is followed by artificial aging at 165 °C for 40 h in the T6 (solution + artificial aging) state. This heat treatment system was specifically developed independently for alloy D2195. The test plates were processed by milling to a size of 300 mm (L) × 150 mm (W) × 6.0 mm (H). The chemical composition of alloy D2195 is listed in Table 1.

Table 1. Chemical composition of D2195 (wt.%).

Component	Cu	Mn	Mg	Ag	Si	Fe	Zr	Li	Al
D2195	3.80	0.0006	0.45	0.30	0.066	0.035	0.12	0.86	Bal.

The microstructure characteristics of alloy D2195 forged specimens after the T6 treatment were obtained using electron backscatter diffraction (EBSD). The microstructure and misorientation angle distribution are depicted in Figure 1. The mechanical properties and grain sizes of the T6 treatment-forged specimens are presented in Table 2.

Table 2. Mechanical properties and grain size of forged plate D2195-T6.

UTS σ_b MPa	YS $\sigma_{0.2}$ MPa	EL %	Average Grain Size/ Standard Deviation μm	Misorientation Angle (2–15°) %	Average Vickers Hardness $H_{V0.5}$
495	422	9.5	10.3/3.9	31.0	156

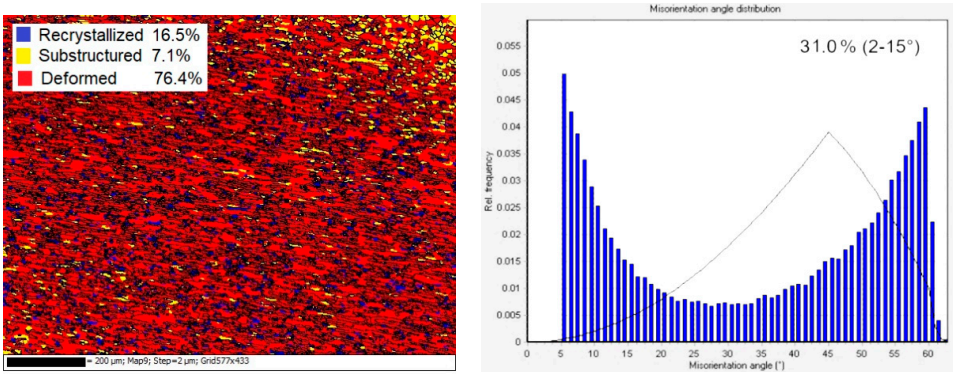

(**a**) (**b**)

Figure 1. (**a**) Microstructure and (**b**) misorientation grain distribution of forged D2195-T6.

2.2. Welding Procedure

Welding test plates were made by manual GTWA process with two-layer welds. The welding conditions and relevant parameters are listed in Table 3. The welding parameters, preheating temperature, joint form, welding sequences, heat input, and other factors were adjusted before the actual welding test to optimize reasonable thermal cycles, to reduce or eliminate various metallurgical defects, and to improve the state of joint microstructure. All the welded test plates were examined using radiographed detection in accordance with the standard of space containers.

Table 3. Welding conditions and main process parameters.

Parameter	Value
Surroundings	Temperature: 22–24 °C, Relative humidity: 40–60%
Welding power source	MILLER Dynasty-700, AC Pulse-TIG,
Operation	Manual welding with two layers
W-Zr electrode	Φ 4 mm, 60° conical fillet
Shielding gas	Pure Ar (99.999%)
Flow rate of shielding gas	16 L/min
Back protective gas	Pure Ar (99.999%), 25 L/min
Preheating	80–90 °C
Groove type	V-95° with 1.5 mm blunt edge
Penetration pass	200–220 A/16.5–17.5 V
Welding speed	130–140 mm/min
Filler pass	180–200 A/17.5–18.5 V
Welding speed	90–100 mm/min
Filler wire	Φ 3.2 mm (details in Table 4)

Table 4. Chemical compositions of filler wire and WM of joint (wt.%).

Component	Cu	Ag	Zr	Ti	Si	Al
Wire	6.44	0.35	0.26	0.35	0.28	Bal.
WM	4.15	0.30	0.20	0.12	0.12	Bal.

To accurately understand the thermal input and thermal cycle of the test plate during the welding process, slots with a depth of 1 mm were marked on the back side of the test plate. These slots were at 4 mm, 6 mm, and 8 mm distances from the center of the weld, as depicted in Figure 2. K-type thermocouples were used in the test, and the measurement range was 0–800 °C with a measurement error of ±5 °C. The thermocouples were calibrated before the test to eliminate the effect of "temperature drift" on the measurement results. The welding thermal cycle curves were recorded to obtain their corresponding temperature histories of the filler pass and analyze the evolution of the

joint microstructure. The temperature experience and corresponding microstructural impact in each zone are also reflected in Figure 3.

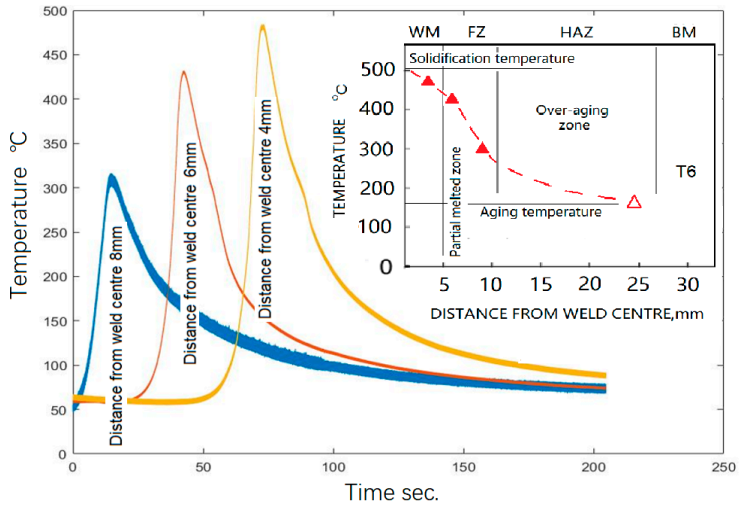

Figure 2. Recorded thermal cycle curves in welding and the local zone conditions.

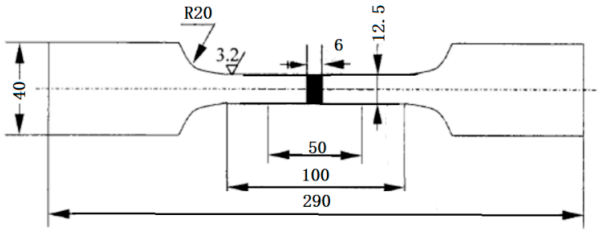

Figure 3. Dimensions of tensile test specimen (in mm).

The test plate and welding fixture were preheated prior to welding to reduce the heat-induced stress and deformation of the test plate.

2.3. Analysis of the Fusion Joint

A special filler wire was designed and developed after many tests for the fusion welding of alloy D2195. The chemical compositions of the filler wire and WM of the joint are listed in Table 4. After welding, a test plate was fabricated to the size specified by the Chinese Standards GB/T 16865-2013 and GB/T2654-2008, with a gauge of 50 mm, as depicted in Figure 3.

To obtain the performance of the fusion joint, tensile and Vickers hardness tests were performed. The fracture location of a typical tensile specimen is shown in Figure 4. The distance from the center of the weld was approximately 15 mm. The Vickers hardness was measured at those locations in the cross section of each joint, which were 1.5 mm and 4.5 mm away from the bottom edge of each test plate, in accordance with the requirements of the "Hardness Test Methods on Welded Joints" (GB/T 16865). Two adjacent points were spaced at 0.5 mm from the center of each joint to the BM. The test loading force was 500 gf and the retention load time was 10 s. The location for the hardness tests is depicted in Figure 5a, and the metallographs and morphologies of the WM and each local zone are depicted in Figures 5b and 5c, respectively.

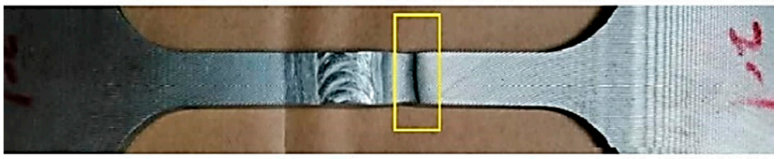

Figure 4. Fracture location of the tensile specimen.

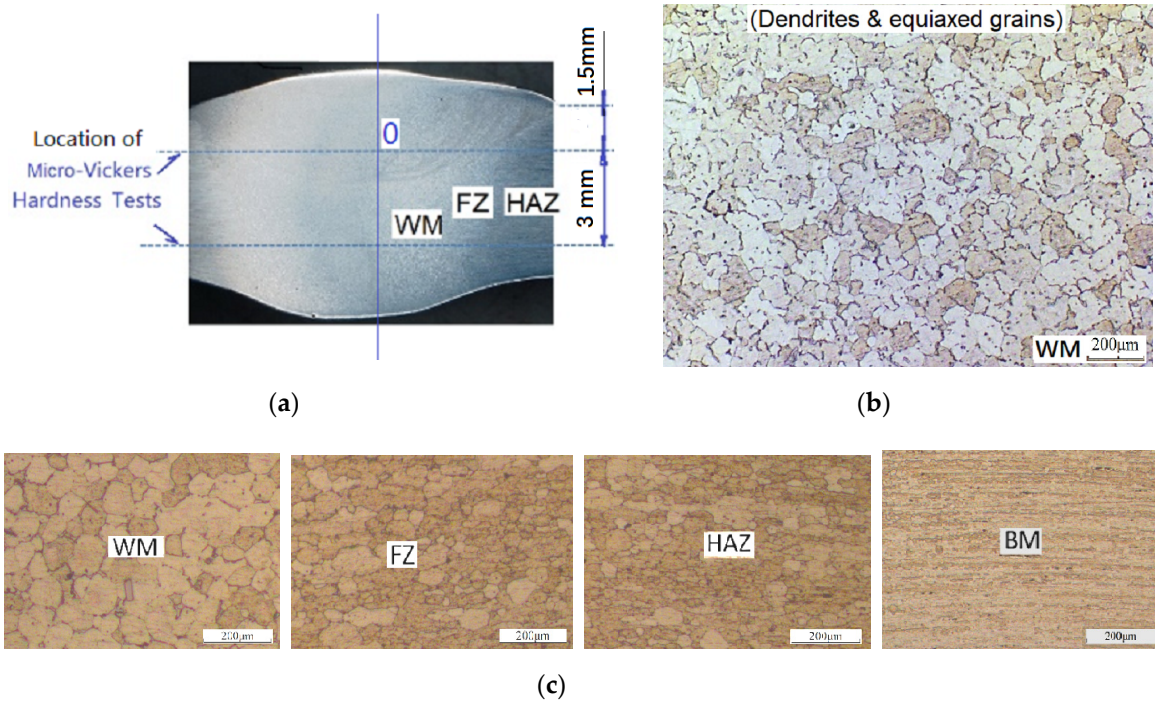

Figure 5. Metallographs and morphologies of the joint with each local zone. (**a**) Location for the hardness tests; (**b**) Microstructure of the WM; (**c**) Metallographs and morphologies of the WM and each local zone.

Figure 6 shows the Vickers hardness distributions from the WM to the BM. All the specimens were welded under the same welding condition as shown in Table 3; samples 1 and 2 are repetitions. The microstructural characteristic quantities of WM, FZ, HAZ, and BM were obtained using EBSD, as depicted in Figure 7. Subsequently, the statistics of the recrystallized grain fraction, grain sizes, misorientation angles, and their distributions were obtained and the corresponding microstructure morphologies were observed and contrasted. In general, the grain size in each local zone of the joint appeared fine and uniform, which is favorable for the suppression or elimination of various types of microcracks during welding.

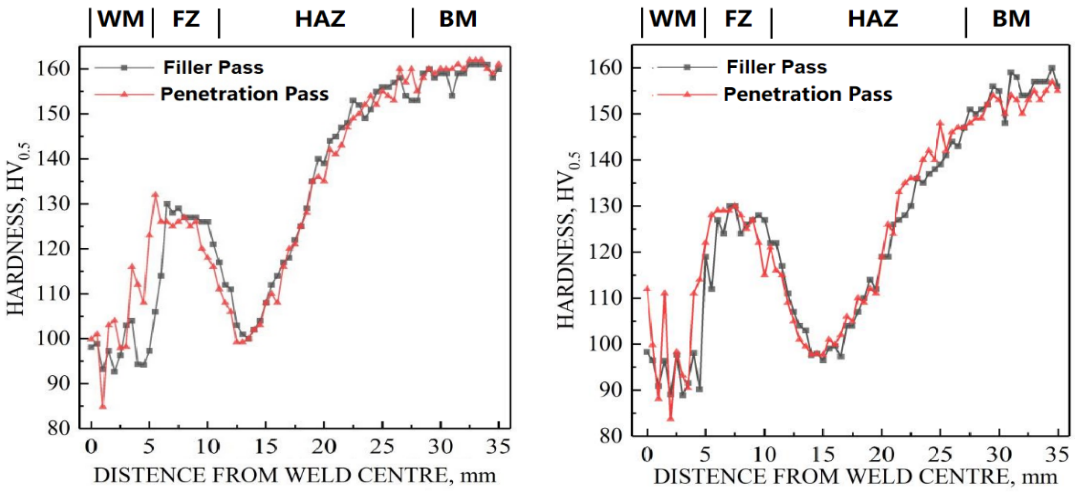

Figure 6. The Vickers hardness distributions from WM to BM: (**a**) sample 1 and (**b**) sample 2.

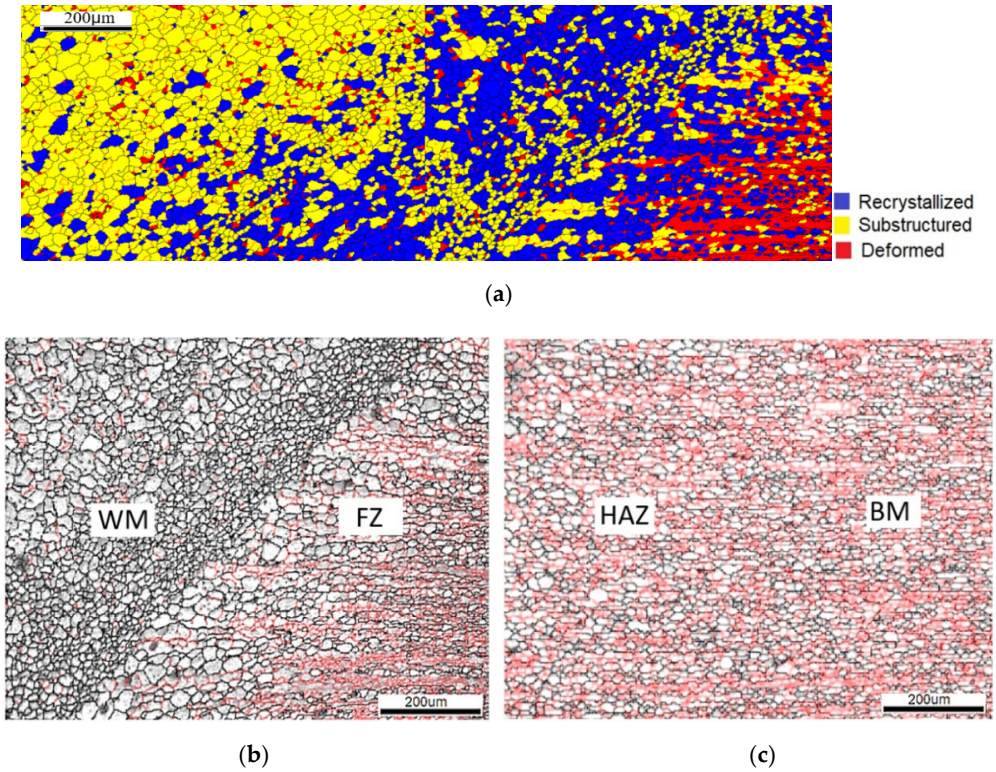

Figure 7. (**a**) Microstructure characteristic quantities of (**b**) joint and (**c**) grain morphologies.

The corresponding temperature histories of thermal cycles at three locations of the joint hardness distributions and microstructure morphologies of various zones indicate the following:

(1) The WM was located at the range of approximately 5 mm from the center of the weld to each side. Because of the V-95°-shape groove, the widths of the front and back joints of the test plate were approximately 10 mm and 8 mm, respectively. While the filler pass was welded, the thermal cycle history of the weld metal at a distance of 4 mm from the weld center can be described as follows: the instantaneous peak temperature was approximately 480 °C and the retention time was approximately 40 s in the range of 180–200 °C. The crystallizing morphology on the WM was dendrites and equiaxed grains with a high substructure grain fraction, and the strengthening element of filler wire compositions formed a limited solid solution effect during the thermal cycle. In addition, dispersive and fine aluminized substance points such as Al_3Zr and Al_3Ti can exist in the WM owing to the peritectic reaction of Zr and Ti in the filler wire (refer to Table 4) during the molten pool crystallization to bring about the effect of refining grains, whose microscopic morphology is shown in Figure 7b.

(2) The weld fusion line is an interface between the WM and HAZ in the fusion joint. In general, the microstructure of the FZ including the fusion line and its two sides would be more complex than that of the other zones of the joint. Under the experimental conditions, the FZ was 5.5–11 mm from the weld center. Because the V-shaped groove had a 1.5 mm blunt edge, there was a dilution rate of 15–20% between the filler wire and BM on the chemical compositions (refer to Table 4) at both sides of the fusion line, so that alloy elements may be interpenetrated and the grain boundary segregation phenomena may occur. Therefore, aspects such as the microstructure and performance of the joint changed significantly in terms of the hardness distribution (Figure 6). The measured instantaneous temperature peaked at approximately 430 °C during a thermal cycle at a location 6 mm from the weld center, and the retention time was approximately 40 s at approximately 150 °C. The recrystallization fraction of the microstructures peaked in this zone. In addition, a local "strengthening" phenomenon appeared because of the climbing and rearrangement of dislocations during the formation of solidified substructures. The micromorphology of the fusion zone is shown in Figure 7a.

(3) The HAZ of the joint was 11.5–27.5 mm from the weld center, whereas the instantaneous temperature peak was at approximately 300 °C and the retention time was approximately 150 °C to result in the BM partially dissolved and produce a softening zone which was about 16 mm wide. Its microstructure retained the originally highly deformed grain fraction of the BM. The metallography of the joint zone is depicted in Figure 7b.

(4) The deformed grain fraction of BM was up to 76.4%, which indicates that significantly high internal energy was stored in the base metal during the forming processes to affect the microstructure of the joint and the evolution of the grain.

3. Analysis Method

3.1. Establishment of an Adaptation Model Based on the Hall–Petch Relation

Understanding the correlation between the microstructure and performance of high-strength Al alloy welded joints is of significance for regulating and optimizing welding processes. Therefore, a quantitative analysis of the process has been a research area since a long time. Generally, the Hall–Petch relationship has been applied for the analysis of the relationship between material microstructures and performances [11,12]. The relationship between the material yield strength (σ_y) and its average grain diameter (d) can be expressed as

$$\sigma_y = \sigma_0 + k_y d^{-1/2} \quad (1)$$

where σ_0 is the friction stress and k_y is a positive yielding constant associated with the stress required to extend the dislocation activity into adjacent unyielded grains. Equation (1) can be reformulated in terms of the hardness, H_v, through the following relation [13,14]:

$$H_v = H_0 + k_H d^{-1/2} \quad (2)$$

where H_0 and k_H are the appropriate constants associated with the hardness measurements. Because σ_0, H_0, and k are chemistry- and microstructure-dependent constants, metallurgical factors such as melting, semimelting, overaging, dissolution softening, and grain coarsening would occur frequently in fusion joints of solid solution strengthened aluminum alloys. It would be difficult to fully express the correlation between the microstructure and performance of the joints of such Al alloys using only characteristic quantities such as the grain size and microhardness. As depicted in Figure 8a, even though a trend in the Hall–Petch relationship is observed, it reflects the effects of multiple microstructure factors on the behavior of the performance [5,15,16]. Some characteristic information that characterizes the joint microstructural evolution should be considered and selected in accordance with the characteristics of the solid solution strengthened Al alloy in the case of fusion welded joints to further participate in and integrate into the analysis of the correlation of joint performances. Therefore, the distributions of the recrystallized grain fraction and misorientation angle of each zone were considered as additional factors; the features are depicted in Figure 8b.

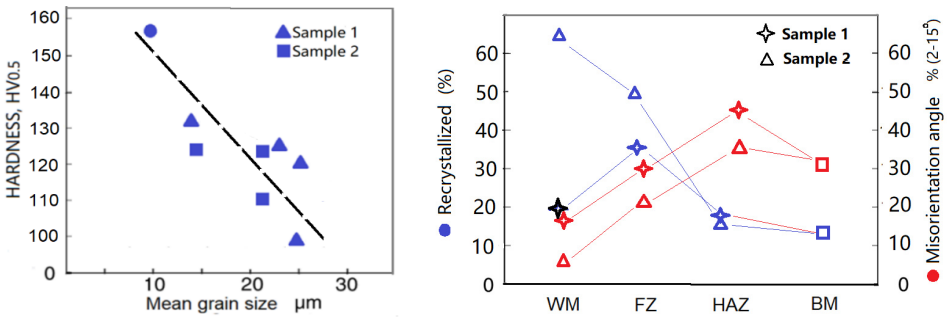

(**a**) (**b**)

Figure 8. (**a**) Trend in H–P relationship and (**b**) distributions of recrystallized grain fraction and misorientation angle of each zone of joints.

Based on the actual measurements of physical samples under certain welding conditions, a corresponding phenomenological statistical model of the evolution of the microstructure has been proposed to evaluate or predict the local performance evolution of welded joint, which is an available research method for thermoforming manufacturing including welding. The analysis of the correlation between the microstructure and performance of a welded joint not only depends on its chemical composition but also relates to the welding thermal cycle-induced microstructure evolution and multiple factors of different attributes, such as the welding process parameters. Therefore, both characteristic quantities, namely, joint recrystallization grain fraction affected directly by the welding thermal cycle and the misorientation angle distribution related to the material mechanical plastic deformation and dislocation climbing behaviors, should be chiefly taken into account based on the statistical analysis model of a few characteristic quantities. The former is related to the microstructure states of WM and FZ, whereas the latter relates to their comprehensive mechanical properties. Additionally, the correlation between the joint microstructure and its performance can be reflected more comprehensively by integrating statistical distributions of the grain size and Vickers hardness of each zone. Therefore, a statistical analysis model for correlation between some characteristic quantities of various attributes and joint performance is proposed.

Based on the multidimensional vector inner product principle of the similar system theory and multiattribute characteristic information, the degree of difference in its multifactor fit (F–fit) was defined as the distance vector ($d_{j,R}$), which is also described as the difference between the statistical value (a_j) and its corresponding reference quantity (b_R) in n characteristic factors. It is equivalent to the distance vector sum ($d_{j,R}$) of various characteristic factors ($a_{j,i}$) and their corresponding reference quantities ($b_{R,i}$). It can be expressed as:

$$d_{j,R} = \|a_j - b_R\| = \sqrt{\sum_{i=1}^{n}\left(a_{j,i} - b_{R,i}\right)^2} \quad (3)$$

The statistical significance of Equation (3) is the standard deviation of the degree of difference between n characteristic factors ($a_{j,i}$) and their corresponding reference quantities ($b_{R,i}$). The continuity of the evolution of joint microstructures is a prerequisite for the selection of a statistical reference, which is the interface of each zone in the metallurgical sense. Therefore, the FZ of a joint is determined as the adaptation reference of its WM and HAZ to conform to the above physical meaning. Similarly, the HAZ serves as an adaptation reference to the BM.

3.2. Calculation of the Fittingness of a Joint Based on Some Characteristic Quantities

Table 5 lists the statistical values that characterize the correlation between structures and performances of each zone of welded joints. Two samples were selected based on the welding conditions (Table 3). Because manual welding may result in some fluctuations in welding, the characteristic quantities (such as the misorientation angle distribution and recrystallized grain fraction) of microstructures of the both samples fluctuated to a certain extent; however, their grain sizes and microhardness were basically not influenced. These cases also reflect the random effects of actual welding conditions on the sample microstructure and performance.

Table 5. Statistical characteristic values of the joint samples.

Distances from Weld Centre (mm) // Local Zone	Recrystallize Fraction %	Misorientation Angle (<15°) %	Average Grain Size μm	Average Vickers Hardness $H_{V0.5}$
0–5//WM1	19.9	18.3	24.9	99
WM2	63.95	6.3	21.4	101
5.5–11.0//FZ1	35.3	29.9	22.3	125
FZ2	49.75	21.5	21.7	123
11.5–27.5//HAZ1	18.9	48.7	25.4	120
HAZ2	18.0	35.5	14.2	132
>28//BM	16.5	30.1	10.3	156

Dimensionless treatment is performed for the ratio of $a_{j,I}$ and $b_{R,I}$; the closer the ratio to 1, the higher the fittingness between the two. Therefore, in Equation (4), where $1 - \frac{a_{j,i}}{b_{R,i}}$ represents the deviation of the ith characteristic quantity and $\frac{\sum_{i=1}^{n} \|1-\frac{a_{j,i}}{b_{R,i}}\|}{n}$ represents the average deviation of the sum of n characteristic quantity deviations. According to the concept of fixed moment, the fittingness was defined as $F \leq 1$. For sample 1, FZ1 acts as its statistical reference value. The fittingness between the WM and FZ of a joint is calculated using Equation (5), where n is equal to 4. The fittingness between the WM and FZ of a joint is:

$$F_{1-1} = 1 - \sqrt{\frac{\sum_{i=1}^{n}\left(1-\frac{a_{j,i}}{b_{R,i}}\right)^2}{n}} \quad (4)$$
$$= 1 - ([(1 - 19.9/35.3)^2 + (1 - 18.3/29.9)^2 + (1 - 24.9/22.3)^2 + (1 - 99/125)2]/4)^{1/2} = 0.69$$

The fittingness between the FZ and HAZ of a joint is:

$$F_{1-2} = 1 - ([(1 - 18.9/35.3)^2 + 1 - 48.7/29.9)^2 + (1 - 25.4/22.3)^2 + (1 - 120/125)^2]/4)^{1/2} = 0.60 \quad (5)$$

HAZ is derived from the evolution of the structure and performance of the BM due to a welding heat cycle. Distributions of grain sizes and hardness indicate that the structures of this zone are significantly sensitive to any change in welding conditions. As mentioned above, HAZ acts as a statistical reference for calculating the fittingness to BM based on the continuity of the evolution of the structure and performance of a joint. For HAZ1, its fittingness is calculated as:

$$F_{1-3} = 1 - ([(1 - 16.5/18.9)^2 + (1 - 30.1/48.7)^2 + (1 - 10.3/25.4)^2 + (1 - 156/120)^2]/4)^{1/2} = 0.61 \quad (6)$$

Similarly, calculation was performed for sample 2 using the same method. Based on the data (Table 4) and statistical calculations, the crystallization speed, component segregation, and other factors may lead to increased uncertainty in the recrystallization fraction, misorientation angle distribution, and other parameters of this zone during the solidification of its joint metal. There is no substantial interference from the comprehensive impact of various influencing factors and effects. For sample 1, the fittingness between WM1 and FZ1, HAZ1 and FZ1, and HAZ1 and BM were 69%, 60%, and 61%, respectively. In contrast, the fittingness between WM2 and FZ2, HAZ2 and FZ2, and HAZ2 and BM were 61%, 51%, and 81% for sample 2, respectively.

The statistical analysis results (shown in Figure 9) of the fittingness between the microstructure and performance of each zone of the joint indicate that their weakened positions can be verified using a quantitative evaluation method for fusion joints of characteristic information after the characteristic quantities of each zone are obtained. Moreover, the effects of the welding process factors can be evaluated. The mechanical properties of the samples are depicted in Figure 9b.

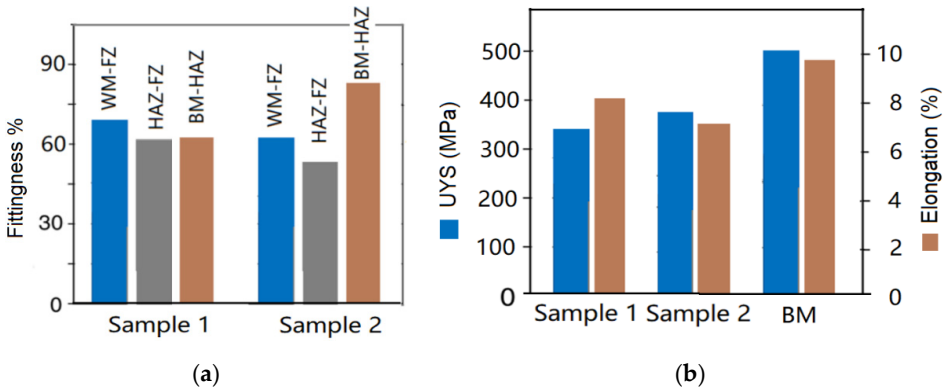

(**a**) (**b**)

Figure 9. (**a**) Results of the statistical analysis of the fittingness between microstructures and performances of each zone of joints and (**b**) mechanical properties of samples.

As for the fusion welded joints of forged D2195 in this study, its welded joints were likely fractured under an external tensile force in the HAZ. The tensile strengths and elongations of samples 1 and 2 were 341 MPa and 8% and 370 MPa and 7%, respectively. Their strength coefficients and elongations were 69%, 75%, 84%, and 74% of those of the BM. The results were consistent with the analysis of their fittingness and prove that the comprehensive performances of forged D2195 joints were superior to those of joints of forged AA2195 fabricated using fusion metallurgy [5].

4. Conclusions

(1) The tensile strength and elongation of forged alloy D2195 joints using GTAW can be up to approximately 70% of those of the BMs fractured in the HAZs. The correlation between the joint microstructure and its performance and the weldability advantages of this type of Al alloy can be more comprehensively reflected by the recrystallization grain fraction, misorientation angle distribution, and the distribution of the grain size and Vickers hardness.

(2) Based on the concept of the Hall–Petch relationship, a statistical analysis model is established using the correlation between the microstructure and performance of several characteristic quantities by integrating the characteristic information of multiple different attributes to deeply understand the comprehensive effects of various zones of welded joints that undergo welding thermal cycles. Thus, the performance of fusion joints under the strong coupling of multiple factors can be quantitatively evaluated.

(3) The statistical calculation results of structures and fittingness between various zones of the forged D2195 joint using GTAW indicate that their weakened positions can be evaluated through a quantitative evaluation method. Thus, a cognitive approach can be adopted to not only optimize joint structures and performances by adjusting the welding processes but also popularize the application advantages of metallurgical characteristics of alloy D2195.

Author Contributions: Conceptualization, C.L. and Y.S.; methodology, formal analysis and writing—review and editing, Y.S.; validation, C.L. and Y.W.; investigation, supervision, and funding acquisition, H.L.; resources and writing—original draft preparation, C.L.; data curation and visualization, L.Y. All authors have read and agreed to the published version of the manuscript.

Funding: The authors gratefully acknowledge the financial support provided by the National Natural Science Foundation of China (Grant No. 51675375), and the project funds support provided by Science and Technology Committee of Sichuan Aerospace Technology Research Institute (Project No. F70319).

Conflicts of Interest: The authors declare no conflict of interest.

References

1. Rioja, R.J.; Liu, J. The evolution of Al–Li base products for aerospace and space applications. *Metall. Mater. Trans. A* **2012**, *A43*, 3325–3337. [CrossRef]
2. Ishchenko, A.Y. High-strength aluminium alloys for welded structures in the aircraft industry. *Weld. Int.* **2005**, *19*, 173–185. [CrossRef]
3. Prasad, N.E.; Gokhale, A.A.; Wahhil, R.J.H. *Aluminum-Lithium Alloys: Processing, Properties, and Applications*; Butterworth-Heinemann: Oxford, UK, 2014; pp. 3–22.
4. Nayan, N.; Narayana Murty, S.V.S.; Mukhopadhyay, A.K.; Prasad, K.S.; Jha, A.K.; Pant, B.; Sharma, S.C.; George, K.M. Ambient and cryogenic tensile properties of AA2195-T87 sheets with pre-aging cold work by a combination of cold rolling and stretching. *Mater. Sci. Eng. A* **2013**, *585*, 475–479. [CrossRef]
5. Abd Elaty, A.; Xu, Y.; Guo, X.; Zhang, S.-H.; Ma, Y.; Chen, D. Strengthening mechanisms, deformation behavior, and anisotropic mechanical properties of Al-Li alloys: A review. *J. Adv. Res.* **2018**, *10*, 49–67. [CrossRef] [PubMed]
6. Huang, C.; Li, H.; Li, J.; Luo, C.; Ni, Y. Residual stress measurement on propellant tank of 2219 aluminum alloy and study on its weak spot. *J. Mech. Sci. Technol.* **2017**, *31*, 2213–2220. [CrossRef]
7. Xu, Q.; Lavernia, E.J. Fundamentals of the Spray Forming Process. In Proceedings of the International Conference on Spray Deposition and Melt Atomization, SDMA 2000, Bremen, Germany, 26–28 June 2000; Volume 1, pp. 17–36.

8. Zhang, Q.; Zhang, C.; Lin, J.; Zhao, G.; Chen, L.; Zhang, H. Microstructure analysis and low-cycle fatigue behavior of spray-formed Al-Li alloy 2195 extruded plate. *Mater. Sci. Eng. A* **2019**, *742*, 773–787. [CrossRef]
9. Wang, X.D.; Pan, Q.L.; Xiong, S.W.; Liu, L.L. Prediction on hot deformation behavior of spray formed ultra-high strength aluminum alloy-A comparative study using constitutive models. *J. Alloys. Compd.* **2018**, *735*, 1931–1942. [CrossRef]
10. Singer, A.R.E. Recent developments in the spray forming of metals. *Int. J. Powder Metal. Powder Technol.* **1985**, *21*, 219–222.
11. Cordero, Z.C.; Knight, B.E.; Schuh, C.A. Six decades of the Hall-Petch effect-A survey of grain-size strengthening studies on pure metals. *Int. Mater. Rev.* **2016**, *61*, 495–507. [CrossRef]
12. Wyrzykowski, J.W.; Grabski, M.W. The Hall-Petch relation in aluminium and its dependence on the grain boundary structure. *Philos. Mag. A* **1986**, *53*, 505–520. [CrossRef]
13. Ito, Y.; Edalati, K.; Horita, Z. High-pressure torsion of aluminum with ultrahigh purity (99.9999%) and occurrence of inverse Hall-Petch relationship. *Mater. Sci. Eng. A* **2017**, *679*, 428–434. [CrossRef]
14. Xu, W.; Dvila, L.P. Tensile nanomechanics and the Hall-Petch effect in nanocrystalline aluminium. *Mater. Sci. Eng. A* **2018**, *710*, 413–418. [CrossRef]
15. Hirata, T.; Oguri, T.; Hagino, H.; Tanaka, T.; Chung, S.W.; Takigawa, Y.; Higashi, K. Influence of friction stir welding parameters on grain size and formability in 5083 aluminum alloy. *Mater. Sci. Eng. A* **2007**, *456*, 344–349. [CrossRef]
16. Naib, S.; De Waele, W.; Štefane, P.; Gubeljak, N.; Hertelé, S. Crack driving force prediction in heterogeneous welds using Vickers hardness maps and hardness transfer functions. *Eng. Fract. Mech.* **2018**, *201*, 322–335. [CrossRef]